*Meteoritics & Planetary Science* 49, Nr 12, 2290–2304 (2014)
doi: 10.1111/maps.12379

## Report

# Eutectic metal + troilite + Fe-Mn-Na phosphate + Al-free chromite assemblage in shock-produced chondritic melt of the Yanzhuang chondrite

Xiande XIE[1*], Ming CHEN[2], Shuangmeng ZHAI[3], and Fuya WANG[1]

[1]Key Laboratory of Mineralogy and Metallogeny, Guangzhou Institute of Geochemistry, Chinese Academy of Sciences, 510640 Guangzhou, China
[2]State Key Laboratory of Isotope Geochemistry, Guangzhou Institute of Geochemistry, Chinese Academy of Sciences, 510640 Guangzhou, China
[3]Key Laboratory of Orogenic Belts and Crustal Evolution, MOE, School of Earth and Space Sciences, Peking University, Beijing 100871, China
[*]Corresponding author. E-mail: xdxie@gzb.ac.cn

*(Received 25 February 2014; revision accepted 29 August 2014)*

**Abstract**–An assemblage with FeNi metal, troilite, Fe-Mn-Na phosphate, and Al-free chromite was identified in the metal-troilite eutectic nodules in the shock-produced chondritic melt of the Yanzhuang H6 meteorite. Electron microprobe and Raman spectroscopic analyses show that a few phosphate globules have the composition of Na-bearing graftonite $(Fe,Mn,Na)_3(PO_4)_2$, whereas most others correspond to Mn-bearing galileiite $Na(Fe,Mn)_4(PO_4)_3$ and a possible new phosphate phase of $Na_2(Fe,Mn)_{17}(PO_4)_{12}$ composition. The Yanzhuang meteorite was shocked to a peak pressure of 50 GPa and a peak temperature of approximately 2000 °C. All minerals were melted after pressure release to form a chondritic melt due to very high postshock heat that brought the chondrite material above its liquidus. The volatile elements P and Na released from whitlockite and plagioclase along with elements Cr and Mn released from chromite are concentrated into the shock-produced Fe-Ni-S-O melt at high temperatures. During cooling, microcrystalline olivine and pyroxene first crystallized from the chondritic melt, metal-troilite eutectic intergrowths, and silicate melt glass finally solidified at about 950–1000 °C. On the other hand, P, Mn, and Na in the Fe-Ni-S-O melt combined with Fe and crystallized as Fe-Mn-Na phosphates within troilite, while Cr combined with Fe and crystallized as Al-free chromite also within troilite.

## INTRODUCTION

Shock-induced melt regions (melt veins or melt pockets) can be observed in many chondritic meteorites (e.g., Fredriksson et al. 1963; Rubin 1985; Stöffler et al. 1991), and melting temperatures of up to 1500 °C or more have been reported by Begemann and Wlotzka (1969), Smith and Goldstein (1977), Chen and Xie (1996), and Xie et al. (2001). The melt regions consist of recrystallizing silicate, oxide, iron-nickel metal, and sulfide, and, sometimes, small amounts of silicate melt glass (Price et al. 1979; Scott 1982; Stöffler et al. 1991; Chen and Xie 1996). Metal and sulfide phases in the chondritic melt were completely molten and occur as rapidly solidified metal-troilite eutectic with dendritic or cellular texture, in which metallic dendrites were enclosed in a troilite groundmass (Scott 1982; Rubin 1985; Chen et al. 1995a, 1995b). The investigation of textures, compositions, and microstructures in the metal-troilite eutectic can be used to construct the postshock thermal histories of chondritic meteorites (Begemann and Wlotzka 1969; Taylor and Heymann 1971; Smith and Goldstein 1977; Scott 1982; Rubin 1985; Chen and Xie 1995; Chen et al. 1995a, 1995b; Leroux et al. 2000; Kong and Xie 2003). The cooling rates deduced from the structures of metal dendrites in

the shock-induced melts of chondrites range from 0.1 to 5000 °C $s^{-1}$ (Scott 1982).

Fe-Mn phosphates typically do not occur in ordinary chondrites (Fuchs 1969; Rubin 1997), but some Fe-Mn phosphates were reported in iron and pallasite meteorites (Olsen and Fredriksson 1966; Bild 1974). Olsen and Steele (1993) reported the discovery of Fe-Mn-Na phosphate $(Na,K)_2(Fe,Mn)_8(PO_4)_6$ within troilite nodules of some IIIAB iron meteorites. They provisionally referred to this mineral as 2:8:6 phosphate due to the absence of X-ray data available for this phase.

Chen and Xie (1996) reported a number of Na-bearing Fe-Mn phosphate inclusions within troilite in some metal-troilite eutectic nodules of the Yanzhuang chondrite. These phosphate inclusions occur as fine-grained spherules with 2–8 μm diameter, and containing 48–58 wt% FeO, 2–5 wt% MnO, 38–40 wt% $P_2O_5$, and up to 4.55 wt% $Na_2O$. On the basis of microprobe analyses, they indicated that only a few grains have the composition of graftonite $(Fe_{2.95}Mn_{0.05})_3(PO_4)_2$, but the majority of the Fe-Mn-Na phosphate grains in Yanzhuang may correspond to the 2:8:6 phosphate $(Na,K)_2(Fe,Mn)_8(PO_4)_6$ as those found in IIIAB iron meteorites by Olsen and Steele (1993).

Olsen and Steele (1997) reported a new Fe-Na phosphate mineral galileiite $NaFe_4(PO_4)_3$ that occurs in troilite nodules in iron meteorites of the IIIA and IIIB groups. Grains of galileiite are very small, generally 10 μm or less. This new mineral contains 49.0 wt% FeO, 3.98 wt% MnO, 40.2 wt% $P_2O_5$, and 5.87 wt% $Na_2O$. It is associated with Ca-free graftonite, chromite and, occasionally, schreibersite.

Semeneko and Perron (2005) reported the presence of coarse glassy Fe-Na phosphate globules (up to approximately 20 μm in diameter) containing microcrystals of chromite (≤1 μm) in melt regions of the Krymka (LL3.1) chondrite. These glassy phosphate globules occur in troilite of some metal-troilite intergrowths. Energy-dispersive X-ray spectroscopic analyses give a composition for the phosphate of (in wt% oxides) 7–11 $Na_2O$, 40–50 FeO, 0.45 MnO, 37–40 $P_2O_5$, and some other minor components. They assumed that this composition is somewhat Na-poor compared to the sodium iron phosphate maricite ($FeNaPO_4$, 17.8 wt% $Na_2O$, 41.3 wt% FeO, and 40.8 wt% $P_2O_5$).

More recently, we studied the mineralogy of a large eutectic metal-troilite nodule in the Yanzhuang chondrite in detail, and found several tens of new Fe-Mn-Na phosphate globules and two chromite crystals in this nodule. In this paper, we report the occurrence of this distinct metal + troilite + Fe-Mn-Na phosphate + Al-free chromite assemblage and discuss the mechanism of its formation.

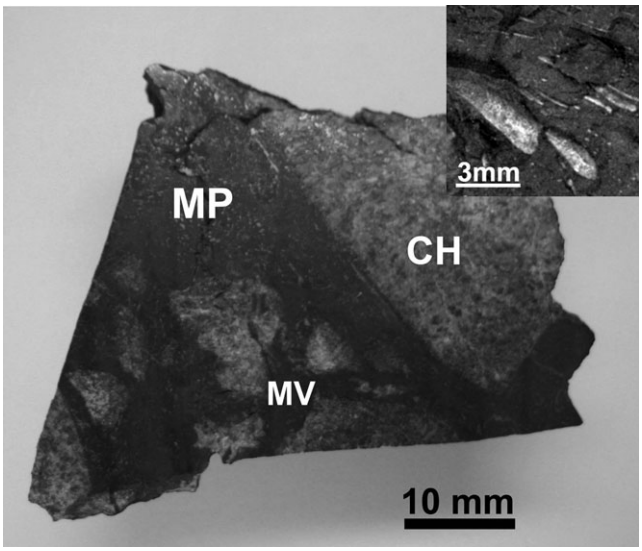


Fig. 1. Cut surface of a large fragment of the Yanzhuang chondrite with melt veins (MV) and melt pockets (MP), and unmelted chondritic host rock (CH). Inset shows metal-troilite intergrowth nodules (white) in the chondritic melt pocket.

## THE YANZHUANG METEORITE

The Yanzhuang meteorite is classified as petrological type H6 chondrite, and considered to be one of the most heavily shocked and severely reheated chondrites described so far (Xie et al. 1991; Begemann et al. (1992); Chen 1992; Kong and Xie 2003; Xie et al. 2011). The meteorite consists of a highly deformed chondritic host and many shock-induced melt veins and melt pockets (Fig. 1). Constituent minerals in the chondritic host comprise olivine, orthopyroxene, clinopyroxene, FeNi metal, troilite, chromite, plagioclase, and whitlockite, in order of abundances (Xie et al. 1994). Melt veins and melt pockets, which connect with each other and penetrate the whole meteorite, make up about 30% of the meteorite. The width of melt veins ranges from 1 to 15 mm, one exceptionally large melt pocket, about 2 × 3 × 4 cm in size, was also encountered in this meteorite (Chen et al. 1995a, 1995b; Chen and Xie 1996). In contrast to the high-pressure mineral-bearing shock veins in some L6 chondrites (Chen et al. 1996, 2003a, 2003b; Sharp et al. 1997; Gillet et al. 2000; Xie et al. 2002, 2011, 2013), the melt veins and pockets in the Yanzhuang H6 chondrite mainly consist of recrystallized microcrystalline olivine and pyroxene, silicate melt glass, and numerous metal-troilite eutectic nodules or inclusions with dendritic texture, whose diameters vary from 0.1 to 10 mm. Some

of the inclusions are elongated (Xie et al. 1994; Chen and Xie 1997; Kong and Xie 2003). The cooling rates during the solidification of dendrites were estimated as 6–30 °C $s^{-1}$ in the interval 950–1400 °C (Chen et al. 1995a, 1995b).

Whitlockite, $Ca_3(PO_4)_2$, is the only phosphate mineral observed in the Yanzhuang unmelted chondritic host. It occurs as irregular grains in the interstices of silicate minerals. The grain size of whitlockite ranges from 0.1 to 0.3 mm. The chemical composition of whitlockite is (in wt% oxide): 45.59 CaO, 4.43 MgO, 2.87 $Na_2O$, 0.07 $K_2O$, 0.04 $Cr_2O_3$, and 46.59 $P_2O_5$ (Chen 1992). Raman spectroscopic analysis indicates that the spectrum of Yanzhuang whitlockite shows five Raman bands at wavenumbers 976, 958, 1086, 602, and 448 $cm^{-1}$ (Chen 1992). This spectrum is almost identical with that of whitlockite in other chondrites (Chen et al. 1995a, 1995b; Xie et al. 2002).

Chromite occurs in the Yanzhuang unmelted chondritic rock as euhedral, subhedral, or irregular grains of 30–80 μm in size. These grains are cracked and fractured. It contains 28.10–29.62 wt% FeO, 2.97–3.41 wt% MgO, 0.92–1.43 wt% MnO, 53.06–55.75 wt% $Cr_2O_3$, and 7.27–8.18 wt% $Al_2O_3$ (Chen 1992).

## SAMPLE AND EXPERIMENTAL TECHNIQUES

Polished thin sections of the Yanzhuang meteorite containing both shock-produced chondritic melt pockets and unmelted chondritic areas were prepared for petrological and mineralogical studies. A large metal-troilite nodule of about 3 × 2.5 mm in size was extracted from a melt pocket of the Yanzhuang meteorite, and used to make a polished section. All polished thin sections were investigated with an optical microscope in reflected light. Chemical compositions of minerals were quantitatively determined with a JEOL JXA-8100 electron microprobe (EPMA) using the wavelength dispersive technique at 15 kV accelerating voltage and beam current of 15 nA for olivine, pyroxene and chromite, and 10 nA for phosphates and feldspathic glass. Natural and synthetic phases of well-known compositions were used as standards, such as albite for $Na_2O$; pyrope for MgO, $Al_2O_3$, and $SiO_2$; apatite for CaO, and $P_2O_3$; magnetite for FeO; rutile for $TiO_2$; pyrite for S; and pure iron and nickel for Fe and Ni, respectively, and the data were corrected using a ZAF program. We carefully chose in the microscope the analytical spots that we analyzed by EPMA to avoid any contamination from other phases. Backscattered electron (BSE) imaging techniques were used to reveal the morphological features of the metal-troilite nodules. Raman spectra of minerals were recorded with a Renishaw *R*-2000 instrument. A microscope was used to focus the excitation beam ($Ar^+$ laser, 514 nm line) to 2 μm wide spots and to collect the Raman signal. Accumulations of the signal lasted 120–150 s. The laser power is 26.8 mW.

The phosphates occurring in the shock-produced metal-troilite nodules of the Yanzhuang meteorite are too small for structure determination by X-ray diffraction. The only way to obtain their structural data is Raman spectroscopy. For this reason, synthesis of phosphates was conducted to compare Raman spectra to natural counterparts. Synthesis of $NaFe_4(PO_3)_2$ and a Fe-Mn-Na phosphate compound was conducted by solid-state reaction. First, stoichiometric proportions of reagent-grade FeO or FeO + MnO, $NH_4H_2PO_4$, and $Na_2CO_3$ powders were mixed. The mixture was ground for 2 h in an agate mortar and pressed into pellets with a diameter of 5 mm under uniaxial pressure of 30 MPa. Second, the pellets were gradually heated from room temperature to 473 K at a rate of 1 K $min^{-1}$ in a gas furnace with an atmosphere of Ar + 1% $H_2$ and kept at 473 K for 2 h. Third, the temperature was increased from 473 K to 973 K at a rate of 60 K $min^{-1}$ and kept at 973 K for 24 h in the same atmosphere of Ar + 1% $H_2$. Finally, the temperature was decreased from 973 K to room temperature in the same atmosphere. The sintered product was ground again and reheated to 973 K for another 24 h in the same atmosphere. The products were analyzed with an X-ray diffractometer using Cu*K*α radiation and a Horiba-JY XploRa Raman spectrometer using an air cooled solid-state laser (532 nm line and 30 mW laser power). The X-ray data were then compared with those of related minerals from RRUFF database (Downs 2006) or the Powder Diffraction File database of the International Centre for Diffraction Data (ICDD PDF).

## RESULTS

### The Chondritic Melt Pocket

The chondritic melt pocket in the Yanzhuang chondrite consists of recrystallized olivine, pyroxene, and silicate melt glass. Figure 2 displays two types of silicate minerals: the coarse-idiomorphic crystals of olivine and low-Ca pyroxene (up to 20–30 μm in length) with interstitial silicate melt glass, and the microcrystalline granular crystals of olivine and pyroxene (only a few μm in size) immersed in silicate melt glass. Tiny metal globules are mainly dispersed within silicate melt glass.

Results of electron microprobe analyses of silicate minerals and melt glass in Yanzhuang melt regions are shown in Table 1. It should be pointed out that olivine in the chondritic melt pocket has the same composition as olivine of the chondritic host, but pyroxene in the

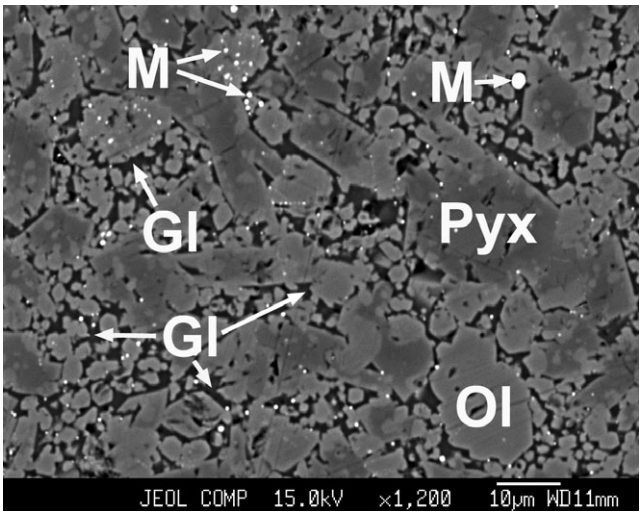


Fig. 2. BSE image showing the mineralogy of the chondritic melt pocket in Yanzhuang. Note the coarse-grained, idiomorphic crystals of low-Ca pyroxene (Pyx) and olivine (Ol) with interstitial silicate melt glass (Gl), and the microcrystalline granular crystals of olivine and pyroxene immersed in silicate melt glass. The small metal globules (M) are dispersed in silicate melt glass.

chondritic melt pocket contains higher contents of $Al_2O_3$, $Cr_2O_3$, CaO, and $Na_2O$ in comparison with pyroxene in the chondritic host.

The chondritic melt pocket of Yanzhuang contains about 5–6% melt glass occurring among the recrystallized silicate minerals (Fig. 2). EPMA measurement shows that the melt glass has a heterogeneous composition (Table 1), corresponding to a quench glass phase.

## The Metal-Troilite Eutectic Nodules

Iron-nickel metal and troilite inside the melt veins and melt pockets of the Yanzhuang meteorite were melted during a shock event, and occur as eutectic metal-troilite nodules of different sizes (Fig. 3). These eutectic nodules display a quench texture composed of dendritic or cellular FeNi enclosed in troilite. The secondary dendrite arm spacing and cell widths of cellular crystals range from 30 to 60 μm. Results of electron microprobe analyses of FeNi metal and troilite in both melt regions and chondritic host are shown in Table 2.

Figure 4 shows a large metal-troilite eutectic nodule (nodule No.1) extracted from a melt pocket of the Yanzhuang meteorite. Metal dendrites in this nodule consist of primary trunks (up to 500 μm in length) with perpendicular secondary branches (up to 100 μm long), while the cellular metal crystals lack secondary dendrite arms. Troilite in this nodule occurs as groundmass filling the spaces between metal dendrites and cells. The metal dendrites and cells in nodule No.1 have quite smooth surfaces while the troilite grains in this nodule were cracked and fractured.

## Fe-Mn-Na Phosphate Globules in the Nodule No. 1

In our recent studies, we observed more than 60 Fe-Mn-Na phosphate globules in the above-mentioned large metal-troilite eutectic nodule No.1. Some of them are shown in Fig. 5 (arrows). The sizes of Fe-Mn-Na phosphate globules range from 2 to 13 μm in diameter. No inclusions of other minerals were observed within the globules.

The phosphate globules mainly have a completely round shape. In addition, globules with drop-like semicircle, ellipsoid, and triangle shapes also occur in this nodule.

Although all observed Fe-Mn-Na phosphate globules occur within troilite, their close relationship with FeNi metal in the nodule is noticeable. According to our statistics, among 45 phosphate globules observed in this nodule, 31 globules (70%) occur in direct contact with dendritic or cellular metal, and only 14 (30%) are completely embedded in troilite.

Table 1. Microprobe analyses of silicates and melt glass in Yanzhuang melt regions (wt%).

| | Ol melt (10) | Ol host (11) | Px melt (11) | Px host (9) | 1 (1) | Glass 2 (1) | 3 (1) |
|---|---|---|---|---|---|---|---|
| $Na_2O$ | n.d. | n.d. | 0.06 | 0.02 | 0.48 | 1.27 | 3.16 |
| $K_2O$ | 0.01 | n.d. | n.d. | n.d. | 5.33 | 0.91 | 0.45 |
| FeO | 16.93 | 16.85 | 10.32 | 10.84 | 11.22 | 5.33 | 3.61 |
| MgO | 42.48 | 42.63 | 30.53 | 30.86 | 21.31 | 9.31 | 6.12 |
| MnO | 0.43 | 0.46 | 0.42 | 0.44 | 4.27 | 3.74 | 0.81 |
| CaO | 0.07 | 0.04 | 1.24 | 0.68 | 1.0 | 2.85 | 3.43 |
| $SiO_2$ | 38.91 | 38.82 | 54.88 | 56.16 | 53.47 | 60.35 | 65.43 |
| $TiO_2$ | 0.04 | 0.04 | 0. 10 | 0.11 | 0.21 | 0.20 | 0.24 |
| $Al_2O_3$ | n.d. | n.d. | 0.64 | 0.20 | 9.41 | 14.88 | 15.98 |
| $Cr_2O_3$ | 0.16 | 0.10 | 0.69 | 0.14 | 0.30 | 0.18 | 0.38 |
| Total | 99.07 | 98.94 | 99.39 | 99.45 | 98.36 | 99.08 | 99.65 |

Ol = olivine; Px = pyroxene; Number in parentheses = number of analyses; n.d. = not detected.

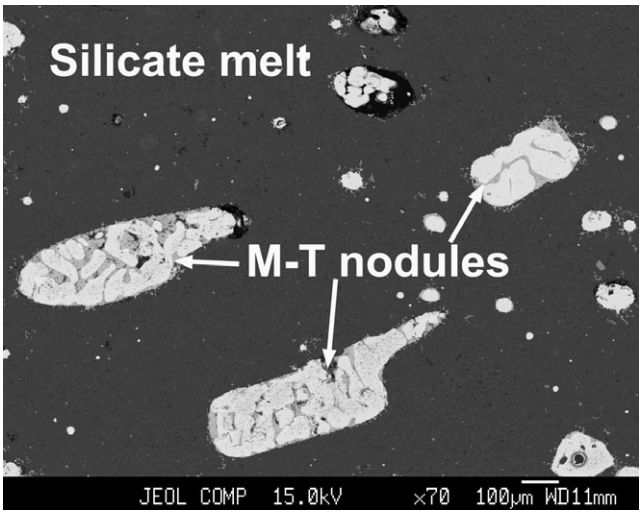


Fig. 3. Backscattered electron (BSE) image showing the metal-troilite (M-T) eutectic nodules of different sizes in the Yanzhuang chondritic melt pocket.

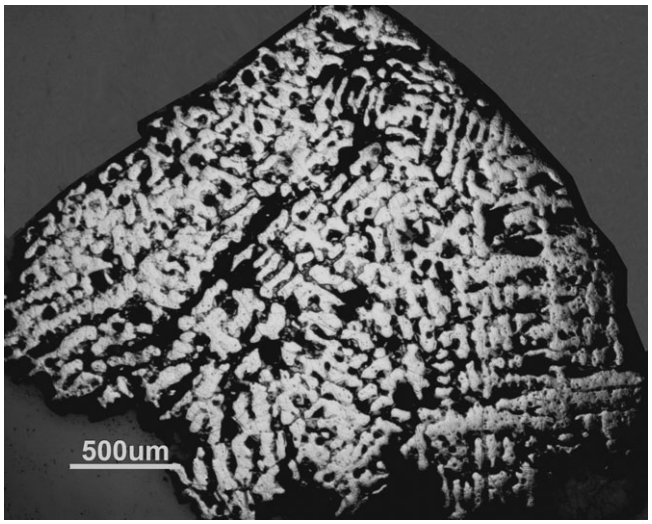


Fig. 4. Cut and polished surface of a large FeNi-FeS eutectic nodule (nodule No.1) extracted from a melt pocket in the Yanzhuang meteorite.

Table 2. Microprobe analyses of FeNi metal and troilite in nodule No.1 (wt%).

| | FeNi melt (9) | FeNi host (5) | Troilite melt (8) | Troilite host (5) |
|---|---|---|---|---|
| Si | 0.01 | n.d. | 0.01 | n.d. |
| Al | n.d. | n.d. | 0.01 | n.d. |
| Co | 0.45 | 0.66 | 0.07 | 0.42 |
| Ni | 7.91 | 6.21 | 0.11 | 0.05 |
| Fe | 90.72 | 92.18 | 62.18 | 60.96 |
| P | 0.54 | 0.01 | n.d. | 1.10 |
| S | 0.02 | 0.10 | 36.48 | 37.14 |
| Mn | 0.01 | 0.03 | 0.02 | 0.03 |
| Cr | 0.13 | 0.32 | 0.14 | 0.07 |
| V | n.d. | n.d. | n.d. | n.d. |
| Ti | 0.02 | n.d. | 0.01 | n.d. |
| Total | 99.81 | 99.12 | 99.03 | 99.74 |

Number in parentheses = number of analyses; n.d. = not detected.

### *Composition of Fe-Mn-Na Phosphate Globules*

Electron microprobe analyses were conducted to investigate the chemical homogeneity of a small phosphate globule G23 in nodule No.1. Three analyses for this globule (Fig. 5d, spots 1–3) show that not only the main components (FeO, MnO, $Na_2O$, and $P_2O_5$), but also the minor components (MgO, CaO, $SiO_2$, and $Cr_2O_3$) are very similar to each other (Table 3), indicating a homogeneous composition.

Among the 45 phosphate globules observed in nodule No.1, only 26 globules (larger than 6 μm in diameter) were measured by EPMA (Table 4). The measured composition of phosphates is similar in $P_2O_5$ content (39–40 wt%) and slightly variable in FeO + MnO contents (52–58 wt%), with varying $Na_2O$ content (from 0.75 wt% for globule G1 up to 6.65 wt% for globule G26).

The EPMA results also show that three phosphate phases can be recognized for the 26 globules in the Yanzhuang nodule No.1: (1) 4 globules (G1–G4) are found to have the composition of Na-bearing graftonite (<1.11 wt% of $Na_2O$) with an empirical formula of $(Fe_{2.72}Mn_{0.13}Na_{0.10}K_{0.01}Ca_{0.01}Cr_{0.01}Si_{0.01})_{2.99}P_{2.02}O_8$, or a simplified formula of $(Fe,Mn,Na)_3(PO_4)_2$ (Table 4); (2) 11 globules (G5–G15) are found to have the composition of galileiite (5.71 wt% of $Na_2O$ in average) and its empirical formula can be written as $(Na_{0.89}K_{0.01}Ca_{0.03}Cr_{0.05})_{0\cdot98}(Fe_{3.61}Mn_{0.29}Mg_{0.02}Si_{0.03})_{3.95}P_{2.99}O_{12}$, or simplified as formula $Na(Fe,Mn)_4(PO_4)_3$ (Table 4); (3) the other 11 globules (G16–G26) give an average composition for the phosphate of (in wt% oxide) 2.71 $Na_2O$, 0.07 $K_2O$, 51.93 FeO, 4.23 MnO, 40.26 $P_2O_5$, 0.01 MgO, 0.05 CaO, 0.11 $SiO_2$, 0.50 $Cr_2O_3$ (Table 4). The empirical formula of this phase (based on 48 O apfu) can be written as $(Na_{1.86.}K_{0.04}Ca_{0.02})_{1.92}(Fe_{15.36}Mn_{1.27}Cr_{0.14}Si_{0.08})_{16.85}P_{12.05}O_{48}$. The simplified formula is $Na_2(Fe,Mn)_{17}(PO_4)_{12}$.

The composition of the third phosphate phase cannot be compared with any of the Fe-Mn-Na phosphates known so far from the literature (Fuchs 1969; Bild 1974; Olsen and Steele 1993, 1997; Rubin 1997; Lodziński and Sitarz 2009). Based on the principles of crystal chemistry, Fe and Mn in the lattice cannot be substituted by Na, Ca, and K (Chen and Xie 1996), so that it is reasonable to assume that this Fe-Mn phosphate with 2.71 wt% of $Na_2O$ might be an unknown Fe-Mn-Na phosphate phase,

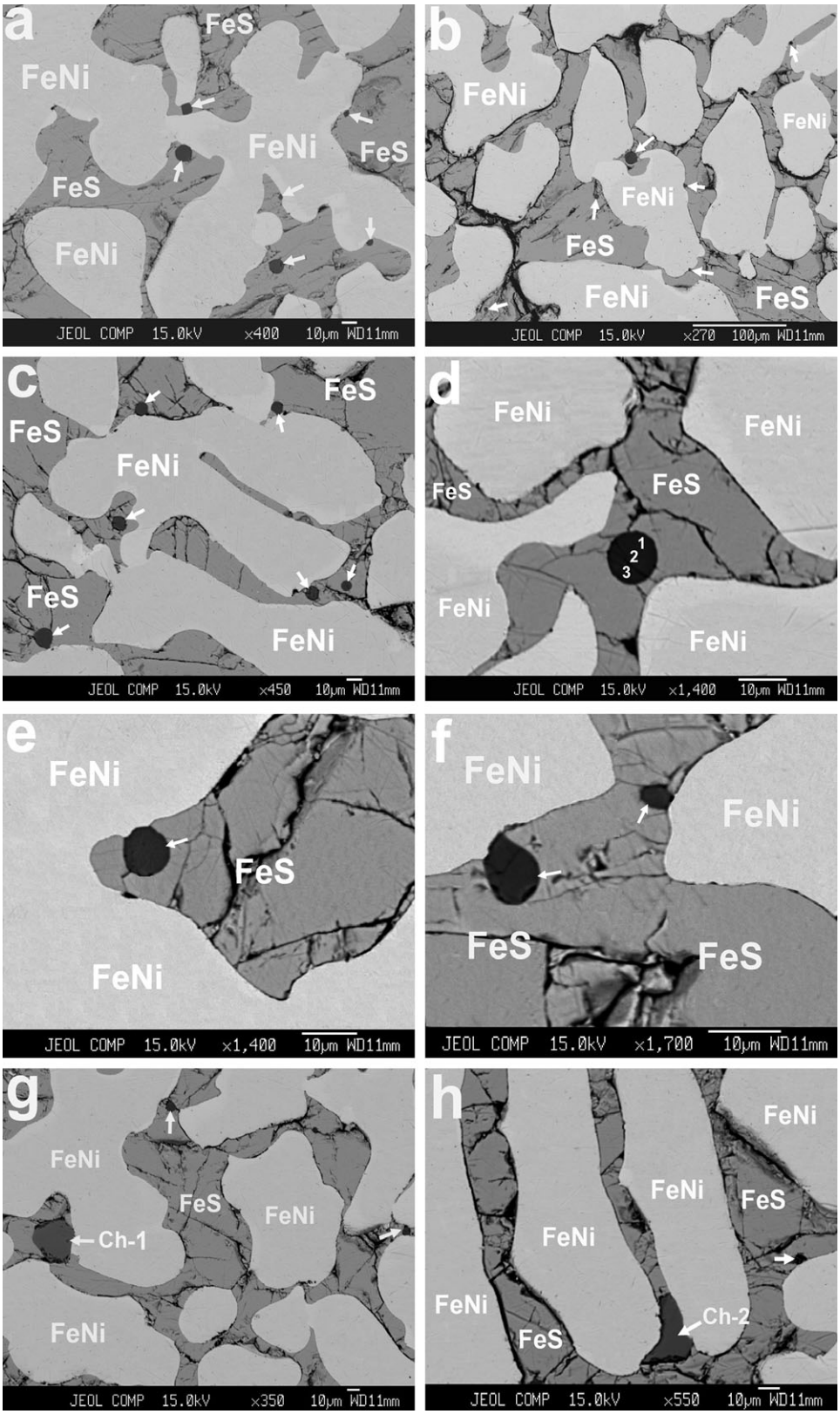


Fig. 5. BSE images showing the occurrences of Fe-Mn-Na phosphate globules within troilite in nodule No.1. a–f) Phosphate globules (indicated by arrows); g) two phosphate globules (arrows) and a euhedral crystal of chromite (Ch-1); and h) a phosphate globule (arrow) with an irregular crystal of chromite (Ch-2).

Table 3. Microprobe analyses of phosphate globule G23 (wt%).

| Points | 1 | 2 | 3 | Ave |
|---|---|---|---|---|
| $Na_2O$ | 5.03 | 5.32 | 5.16 | 5.17 |
| $K_2O$ | 0.12 | 0.16 | 0.13 | 0.14 |
| FeO | 49.86 | 49.57 | 49.69 | 49.71 |
| MgO | 0.15 | 0.14 | 0.16 | 0.15 |
| MnO | 3.59 | 3.95 | 3.50 | 3.68 |
| CaO | 0.35 | 0.31 | 0.49 | 0.38 |
| $SiO_2$ | 0.47 | 0.36 | 0.32 | 0.38 |
| $TiO_2$ | 0.04 | 0.04 | n.d. | 0.03 |
| $Al_2O_3$ | 0.06 | 0.02 | 0.02 | 0.03 |
| $Cr_2O_3$ | 0.86 | 0.83 | 0.82 | 0.84 |
| $P_2O_5$ | 40.00 | 40.18 | 40.52 | 40.23 |
| Total | 100.53 | 100.88 | 100.81 | 100.74 |

n.d. = not detected.

rather than a mixture of Na-bearing graftonite and galileiite.

### *Raman Spectra of Fe-Mn-Na Phosphate Globules*

Raman spectra of Fe-Mn-Na phosphate globules in the Yanzhuang nodule No.1 show rather sharp bands in the region of 950–1130 $cm^{-1}$ (Fig. 6, Fig. 7, and Fig. 8), which is in accordance with the characteristic bands of these phosphates (Burba and Frech 2006; Lodziński and Sitarz 2009). The intense Raman band at 950–980 $cm^{-1}$ can be assigned to the $\nu_1$ symmetric stretching vibration of the $PO_4$ group, while the band at 1035–1130 $cm^{-1}$ corresponds to the $\nu_3$ asymmetric stretching vibration of the $PO_4$ group. Bands at 550–560 and 600–635 $cm^{-1}$ are associated with the $\nu_4$ bending mode, and those at <420–430 $cm^{-1}$ with the lattice

Table 4. Microprobe analyses of phosphate globules in the Yanzhuang nodule No.1 (wt%).

| Globule number | $Na_2O$ | $K_2O$ | FeO | MgO | MnO | CaO | $SiO_2$ | $TiO_2$ | $Al_2O_3$ | $Cr_2O_3$ | $P_2O_5$ | Total |
|---|---|---|---|---|---|---|---|---|---|---|---|---|
| Graftonite | | | | | | | | | | | | |
| G1 | 0.75 | 0.17 | 54.52 | 0.13 | 2.67 | 0.10 | 0.39 | n.d. | 0.02 | 0.29 | 40.29 | 99.33 |
| G2 | 0.84 | 0.13 | 54.71 | 0.13 | 2.43 | 0.11 | 0.39 | n.d. | 0.01 | 0.28 | 39.79 | 99.90 |
| G2 | 0.90 | 0.17 | 55.93 | 0.05 | 2.40 | 0.11 | 0.04 | n.d. | n.d. | 0.19 | 40.36 | 100.15 |
| G4 | 1.11 | 0.21 | 53.63 | 0.05 | 2.63 | 0.10 | 0.11 | 0.04 | n.d. | 0.29 | 29.77 | 99.26 |
| Average | 0.90 | 0.17 | 54.70 | 0.19 | 2.53 | 0.11 | 0.23 | 0.01 | 0.01 | 0.26 | 40.10 | 99.11 |
| Grt* | – | | 58.0 | <0.01 | 1.8 | <0.03 | | | | | 40.8 | 100.6 |
| New phase | | | | | | | | | | | | |
| G5 | 2.24 | 0.09 | 47.96 | 0.01 | 8.06 | 0.01 | 0.05 | n.d. | n.d. | 1.10 | 39.90 | 99.42 |
| G6 | 2.38 | 0.04 | 53.72 | n.d. | 2.97 | n.d. | 0.12 | n.d. | n.d. | 0.39 | 40.76 | 100.38 |
| G7 | 2.40 | 0.08 | 54.27 | n.d. | 2.26 | 0.01 | 0.08 | n.d. | n.d. | 0.42 | 39.87 | 99.39 |
| G8 | 2.54 | 0.08 | 50.00 | n.d. | 6.47 | 0.01 | 0.06 | n.d. | n.d. | 0.54 | 39.51 | 99.21 |
| G9 | 2.59 | 0.07 | 53.24 | n.d. | 3.04 | 0.02 | 0.10 | n.d. | n.d. | 0.34 | 39.85 | 99.25 |
| G10 | 2.66 | 0.08 | 51.91 | n.d. | 3.80 | 0.01 | n.d. | n.d. | n.d. | 0.48 | 40.66 | 99.60 |
| G11 | 2.76 | 0.08 | 51.53 | n.d. | 5.91 | n.d. | 0.13 | n.d. | n.d. | 0.43 | 40.42 | 101.26 |
| G12 | 2.77 | 0.08 | 53.72 | 0.05 | 2.57 | 0.08 | 0.19 | 0.02 | 0.01 | 0.30 | 41.00 | 100.79 |
| G13 | 2.79 | 0.05 | 52.16 | n.d. | 4.27 | 0.02 | 0.10 | n.d. | n.d. | 0.53 | 39.86 | 99.78 |
| G14 | 3.24 | 0.04 | 52.62 | n.d. | 3.74 | 0.03 | 0.08 | n.d. | n.d. | 0.39 | 39.96 | 100.10 |
| G15 | 3.43 | 0.11 | 50.09 | 0.05 | 3.45 | 0.35 | 0.28 | n.d. | n.d. | 0.55 | 41.10 | 99.41 |
| Average | 2.71 | 0.07 | 51.93 | 0.01 | 4.23 | 0.05 | 0.11 | n.d. | n.d. | 0.50 | 40.26 | 99.87 |
| Galileiite | | | | | | | | | | | | |
| G16 | 4.62 | 0.19 | 46.03 | 0.16 | 5.23 | 0.27 | 0.42 | 0.02 | 0.02 | 1.21 | 41.82 | 99.99 |
| G17 | 4.83 | 0.13 | 50.27 | 0.14 | 2.90 | 0.34 | 0.31 | 0.01 | n.d. | 0.30 | 40.68 | 99.91 |
| G18 | 4.83 | 0.16 | 49.38 | 0.14 | 3.63 | 0.18 | 0.42 | n.d. | 0.02 | 0.68 | 40.26 | 99.70 |
| G19 | 4.86 | 0.17 | 51.69 | 0.14 | 2.42 | 0.33 | 0.39 | n.d. | n.d. | 0.69 | 39.89 | 100.58 |
| G20 | 4.86 | 0.14 | 49.59 | 0.06 | 4.13 | 0.45 | 0.17 | n.d. | 0.02 | 0.55 | 40.24 | 100.21 |
| G21 | 4.98 | 0.12 | 50.59 | 0.14 | 3.04 | 0.36 | 0.29 | 0.03 | n.d. | 0.29 | 40.41 | 100.24 |
| G22 | 5.23 | 0.18 | 49.10 | 0.19 | 3.20 | 0.49 | 0.55 | n.d. | 0.04 | 0.54 | 39.94 | 99.46 |
| G23 | 5.32 | 0.16 | 49.57 | 0.14 | 3.95 | 0.31 | 0.36 | 0.04 | 0.02 | 0.83 | 40.18 | 100.88 |
| G24 | 5.39 | 0.19 | 47.28 | 0.22 | 4.80 | 0.64 | 0.60 | n.d. | 0.01 | 1.01 | 40.72 | 99.86 |
| G25 | 5.83 | 0.13 | 50.91 | 0.16 | 3.11 | 0.31 | 0.35 | n.d. | 0.01 | 0.57 | 38.28 | 100.66 |
| G26 | 6.65 | 0.21 | 46.01 | 0.01 | 6.09 | 0.09 | 0.20 | n.d. | 0.04 | 1.55 | 39.43 | 100.40 |
| Average | 5.21 | 0.16 | 49.13 | 0.14 | 3.86 | 0.34 | 0.36 | n.d. | 0.02 | 0.75 | 40.17 | 100.14 |
| Gal** | 5.87 | 0.04 | 49.0 | | 3.98 | | | | | 0.07 | 40.2 | 99.16 |

Grt* = graftonite in Bear Creek iron meteorite (Bild 1974); Gal** = galileiite within troilite nodules in iron meteorites (Olsen and Steele 1997); n.d. = not detected.

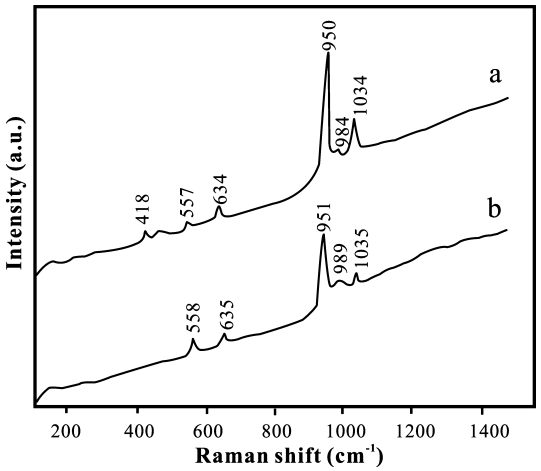


Fig. 6. Raman spectra of Na-bearing graftonite globules in Yanzhuang nodule No.1. a) Globule G2; b) Globule G3.

modes. It must be pointed out that the Raman spectra of all phosphate globules in the Yanzhuang nodule No.1 are typical for an orthophosphate structure, as no Raman band is visible in the region between 700 and 850 $cm^{-1}$, which is generally typical for a polyphosphate structure (Antenucci et al. 1993). The sharp Raman bands obtained from all globules in nodule No.1 indicate that phosphates of these globules are not glassy but crystalline phases.

Corresponding to the compositional differences of phosphate globules in the Yanzhuang nodule No.1, three different groups of Raman spectra can be distinguished for the measured 26 globules: (1) the Na-bearing graftonite shows an intense band at 950–951 $cm^{-1}$, a less intense band at 1034–1035 $cm^{-1}$, and three weak bands at 984–989, 634–635, and 557–558 $cm^{-1}$ (Fig. 6); (2) the Na-rich phosphate galileiite displays an intense band at 980–982 $cm^{-1}$, a broad band at 1124–1129 $cm^{-1}$, and three weak bands at 596–599, 554–558, and 416–417 $cm^{-1}$ (Fig. 7); (3) the possible new phase $Na_2(Fe,Mn)_{17}(PO_4)_{12}$ shows an intense band at 977–978 $cm^{-1}$ with a shoulder band at 940–941 $cm^{-1}$, three weak bands in the region of 1041–1126 $cm^{-1}$, and four weak bands at 605–608, 552–553, 467–471, and 424–425 $cm^{-1}$ (Fig. 8). The reappearance of all Raman spectra for each of the three Fe-Mn-Na phosphate phases in nodule No.1 is fairly good. This may indicate three distinct minerals.

The intense Raman band for the Na-bearing graftonite is at 950–951 $cm^{-1}$, which is a little different from that at 965–968 $cm^{-1}$ for Na-free graftonites (Lodziński and Sitarz 2009). On the basis of a vibrational spectroscopic investigation of structurally related $FePO_4$, $NaFePO_4$, and $LiFePO_4$ compounds, Burba and Frech (2006) indicated that the intense Raman band of $FePO_4$ is at 960 $cm^{-1}$, while that of

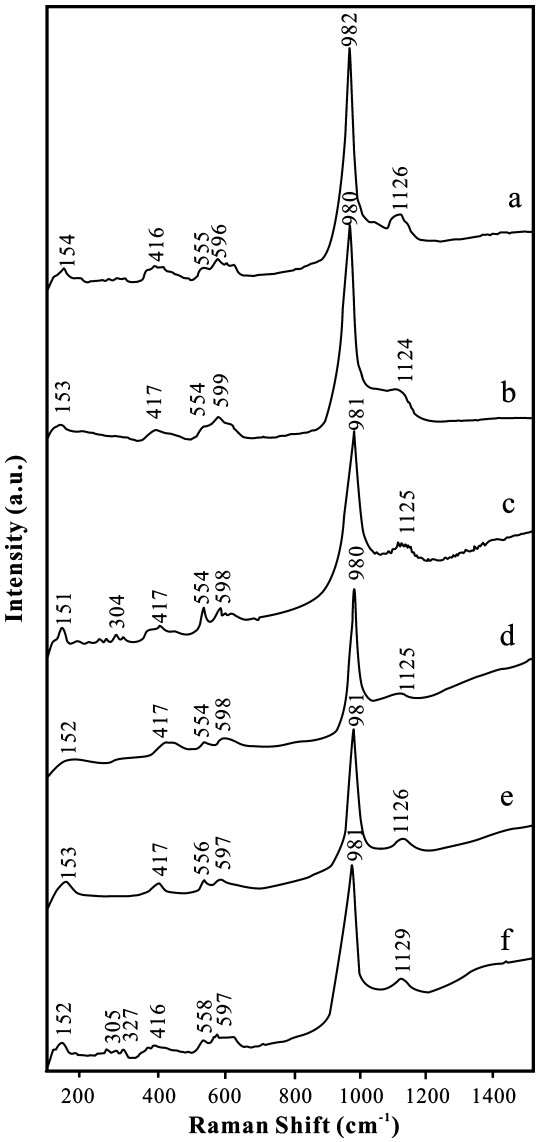


Fig. 7. Raman spectra of galileiite globules in Yanzhuang nodule No.1. a) Globule G16; b) Globule G18; c) Globule G19; d) Globule G22; e) Globule G24; f) Globule G25.

$NaFePO_4$ and $LiFePO_4$ is shifted to 950 $cm^{-1}$, and the $FePO_4$ bands at 1123, 1078, 1062, and 911 $cm^{-1}$ have completely disappeared in the Raman spectra of $NaFePO_4$ and $LiFePO_4$. Hence, it seems reasonable to assume that the insertion of $Na^{1+}$ and $Li^{1+}$ into $FePO_4$ would produce marked changes in the vibration mode of the $PO_4^{3+}$. This result may explain the difference in Raman spectra between the Na-bearing and the Na-free graftonites.

The Raman spectra of the phosphate phase $Na_2(Fe,Mn)_{17}(PO_4)_{12}$ shown in Fig. 8 are different from those of Na-bearing graftonite and galileiite in Yanzhuang in the following aspects: (1) the intense 977 $cm^{-1}$ band of

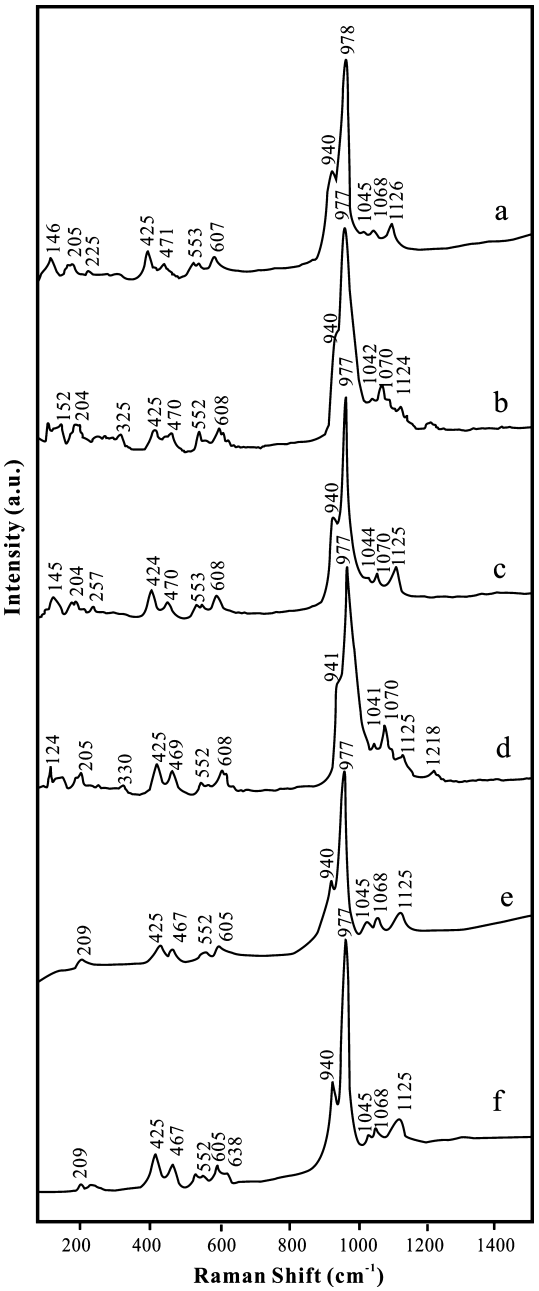


Fig. 8. Raman spectra of $Na_2(Fe_{16}Mn_1)_{17}(PO_4)_{12}$ globules in Yanzhuang nodule No.1. a) Globule G6; b) Globule G10; c) Globule G13; d) Globule G14; e) Globule G15; f) Globule G16.

this phase is much sharper than the intense 950 and 981 $cm^{-1}$ bands of the other two phosphates, respectively, and, furthermore, this band has a shoulder at 940 $cm^{-1}$, which is absent for the other two; (2) in the region between 1041 and 1126 $cm^{-1}$, this phase shows three to four bands at 1044, 1070, 1125, and 1218 $cm^{-1}$, while the other two phosphates only have one or two bands, i.e., the 984 and 1034 $cm^{-1}$ bands for graftonite, and 1125 $cm^{-1}$ band for galileiite; (3) in the region between 400 and 610 $cm^{-1}$, this phase shows four rather sharp Raman bands at 608, 552, 470, and 425 $cm^{-1}$, while the other two phosphates only have two to three weak and broad bands, i.e., the 634 and 557 $cm^{-1}$ bands for graftonite and the 598, 555, and 417 $cm^{-1}$ bands for galileiite. Therefore, this phase may not be a mixture of graftonite and galileiite, but rather an unknown Fe-Mn-Na phosphate phase.

### *Synthesis of Fe-Mn-Na Phosphates*

In order to obtain structural data for the above-mentioned three phosphates in nodule No.1, compounds of the $Fe_3(PO_4)_2$, $NaFe_4(PO_4)_3$, and $Na_2(Fe,Mn)_{17}(PO_4)_{12}$ compositions were synthesized according to the following three solid-state reactions:

$$3FeO + 2NH_4H_2PO_4 \rightarrow Fe_3(PO_4)_2 + 2NH_3 + 3H_2O,$$

$$4FeO + 3NH_4H_2PO_4 + 0.5Na_2CO_3 \rightarrow NaFe_4(PO_4)_3 + 3NH_3 + 0.5CO_2 + 4.5H_2O,$$

$$16FeO + MnO + 12NH_4H_2PO_4 + +Na_2CO_3 \rightarrow Na_2(Fe_{16}Mn)_{17}(PO_4)_{12} + 12NH_3CO_2 + 18H_2O.$$

The three synthesized phosphates were confirmed by X-ray diffraction data. The product of the first reaction only gives diffraction lines typical for graftonite ($Fe_3[PO_4]_2$) at (in Å, the values in parentheses indicate relative intensity): 4.292 (20), 3.652 (15), **3.430 (100),** 3.171 (20), 3.021 (30), 2.918 (35), 2.908 (35), **2.843 (95)**, 2.794 (30), **2.731 (85)**, 2.662 (20), 2.513 (25), 2.420 (30), 2.351 (20), 2.297 (20), etc. (refer to the ICDD PDF 830801 for $Fe_3[PO_4]_2$).

The powder X-ray diffraction patterns of the other two synthesized samples are shown in Figure 9. The X-ray diffraction pattern of the second reaction product (Fig. 9a) shows that besides the main diffraction lines typical for galileiite ($NaFe_4[PO_4]_3$) at (in Å): 3.479 (20), 3.219 (40), **3.021 (100)**, 2.831 (40), **2.712 (70)**, **2.561 (65)**, 1.653 (20), and 1.606 (30) (refer to Table 1 in Olsen and Steele 1997), there are also diffraction lines at **8.132 (50)**, 6.150 (20), 4.271 (10), 4.071 (10), 3.479 (20), **3.109 (40)**, 2.891 (30), 2.830 (30), **2.709 (60)**, 2.601 (30), 2.531 (15), 2.112 (10), 1.976 (25), and 1.830 Å (20). These extra lines can be compared with the main calculated lines in the ICDD PDF 780784 for sodium iron phosphate $NaFe_3(PO_4)_3$, or with those of the mineral alluaudite, $(Na,Ca)(Mn,Mg,Fe^{2+})(Fe^{3+},Mn^{2+})_2(PO_4)_3$ (refer to the X-ray data of RRUFF ID: R100070).

Similarly, the X-ray diffraction pattern of the third reaction product (Fig. 9b) also shows some diffraction lines of sodium iron phosphate $NaFe_3(PO_4)_3$ at (in Å):

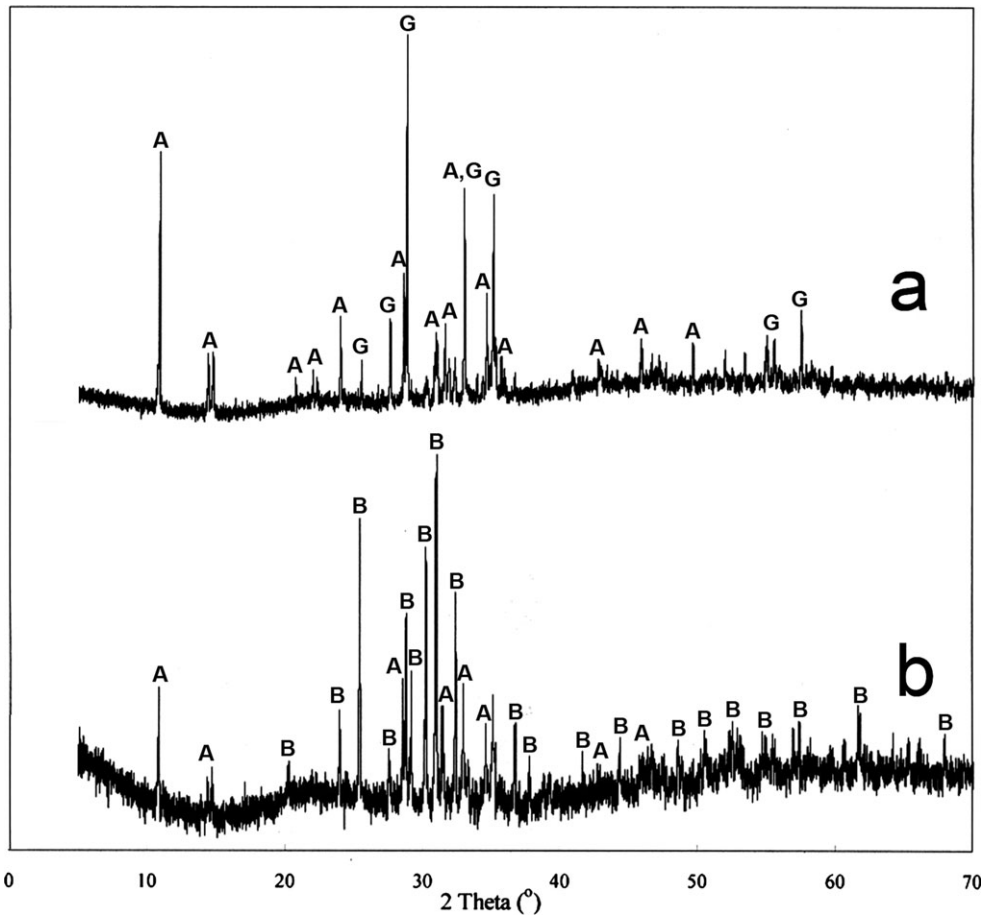


Fig. 9. X-ray diffraction patterns of two synthetic phosphate samples. a) Mixture of galileiite (G) and a sodium iron phosphate of $NaFe_3(PO_4)_3$ composition (A); b) a new phase of $Na_2(Fe_{16}Mn_1)_{17}(PO_4)_{12}$ composition (B) with minor sodium iron phosphate of $NaFe_3(PO_4)_3$ composition (A).

**8.132 (30)**, 6.150 (10), **3.107 (30),** 2.833 (25), **2.710 (30)**, 2.600 (25), 2.112 (10), and 1.975 (10), but the main diffraction lines of this product are at (in Å): 4.378 (10), 3.706 (30), **3.497 (80)**, 3.234(20), 3.101 (60), 3.058 (40), 2.954 (70), **2.884 (100)**, 2.844 (30), 2.760 (60), 2.552 (30), 2.446 (25), 2.380 (20), 2.166 (15), 2.090 (20), 1.873 (15), 1.805 (15), 1.760 (15), 1.668 (10), 1.604 (15), and 1.544 (20). As neither of these main diffraction lines belongs to graftonite, galileiite, and some other Fe- and Fe-Na phosphates (refer to the X-ray diffraction data of RRUFF ID R070553 for sarcopside, $Fe_3[PO_4]_2$; R070273 for maricite, $NaFePO_4$; and R070298 for arrojadite, $Na_2Fe^{2+}[CaNa_2]Fe^{2+}{}_{13}Al[PO_4]_{11}[PO_3OH][OH]_2$), it might belong to a new phosphate phase of $Na_2(Fe,Mn)_{17}(PO_4)_{12}$ composition.

Raman spectra of the new phase and galileiite were measured in the range of 800–1400 $cm^{-1}$. The Raman spectrum of synthesized galileiite shows an intense band at 978 $cm^{-1}$ and a weak band at 1118 $cm^{-1}$ (Fig. 10a) and that of the possible new phosphate phase shows an intense band at 975 $cm^{-1}$ with a shoulder at 933 $cm^{-1}$, and three other bands at 1047, 1070, and 1121 $cm^{-1}$ (Fig. 10b). These data are consistent with natural galileiite and the phosphate phase of $Na_2(Fe,Mn)_{17}(PO_4)_{12}$ composition in Yanzhuang melt pocket.

## Al-Free Chromite Crystals in the Nodule No. 1

The Yanzhuang chondritic portion contains <1 vol% of chromite. The chromite grains contain abundant fractures and cracks. Our recent study revealed that neither residual chromite fragments, nor microcrystals of chromite were observed within the Yanzhuang chondritic melt pocket. However, two chromite crystals were found within troilite and between two neighboring FeNi dendrite arms in nodule No.1. Figure 5g shows a coarse euhedral chromite crystal (Ch-1) of 45 × 40 $\mu m^2$ in size, which coexists with two phosphate globules included in troilite. Figure 5h illustrates another chromite crystal of irregular shape (Ch-2), with a grain size of 40 μm long and 35 μm

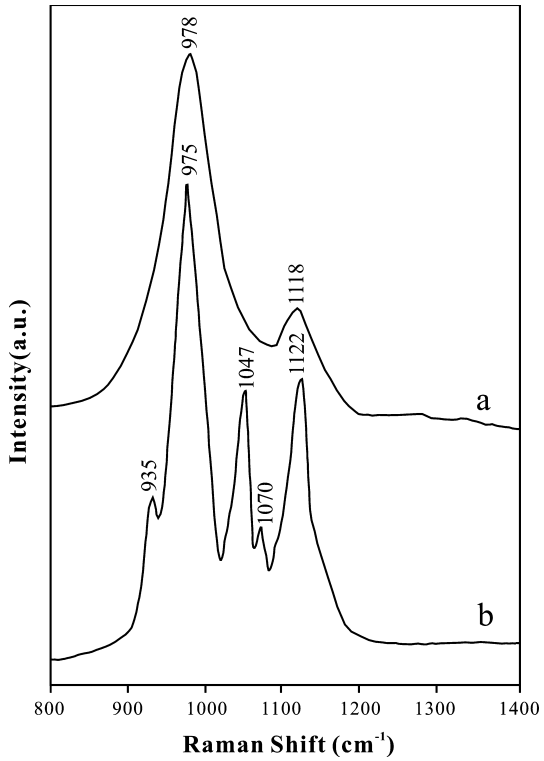


Fig. 10. Raman spectra of two synthetic phosphates. a) Synthetic galileiite; b) synthetic phosphate of $Na_2(Fe_{16}Mn_1)_{17}(PO_4)_{12}$ composition.

wide, which coexists with a phosphate globule within troilite. The surface of both chromite crystals is smooth, and neither fractures nor inclusions were observed within them.

### *Composition of Al-Free Chromite in Nodule No.1*

Electron microprobe measurements were conducted for the chromite crystals Ch-1 and Ch-2 on three and two different points, respectively (Table 5). From the compositional data, the empirical formula of these two chromite crystals in nodule No.1 can be written as $(Fe_{1.00}Mn_{0.02}Mg_{0.01})_{1.03}(Cr_{1.94}V_{0.03})_{1.97}O_4$, which is very close to the ideal formula of $FeCr_2O_4$. Interestingly, the results also show that both chromite crystals are Al-free and similar in contents of main components (FeO and $Cr_2O_3$) and minor components (MnO and $V_2O_3$), although these two crystals occur in different areas in nodule No.1.

Comparing with the composition of chromite in the Yanzhuang chondritic host ($[Fe_{0.84}Mg_{0.14}Mna_{0.03}Ca_{0.01}]_{1.02}[Cr_{1.50}Al_{0.33}Si_{0.08}Ti_{0.03}V_{0.02}]_{1.96}O_4$) (Table 5, last column), chromites in nodule No.1 contain higher contents of FeO (32.29 versus 28.87 wt%) and much higher contents of $Cr_2O_3$ (65.95 versus 54.95 wt%), but the contents of all other minor components, such as MgO, CaO, MnO, $SiO_2$, and $TiO_2$, markedly decreased. It should be pointed out that the chromite in Yanzhuang chondritic host contains 7.98 wt% of $Al_2O_3$, whereas the chromite crystals in nodule No.1 do not contain any $Al_2O_3$. This indicates that the Al-free chromite in nodule No.1 must be formed by crystallization in the shock-produced Fe-Ni-S liquid.

### *Raman Spectra of Al-Free Chromite in Nodule No.1*

Raman spectra of chromites generally show three characteristic main bands in the region of 480–690 $cm^{-1}$ (Xie et al. 2001; Chen et al. 2002; Semeneko and Perron 2005). The Raman spectra of two chromite grains in nodule No.1 are quite similar, displaying an intense band at 680–681 $cm^{-1}$, and two bands at 497–500, and 598–600 $cm^{-1}$ (Fig. 11b and 11c). These Raman spectra are also similar to that of chromite in Yanzhuang chondritic host (Fig. 11a), but the 680–681 $cm^{-1}$ band of chromites in nodule No.1 is much sharper than that

Table 5. Electron microprobe analyses of chromite in the Yanzhuang nodule No.1.

| Sample number | Ch-1a | Ch-1b | Ch-1c | Ch-2a | Ch-2b | Ave | Chromite in meteorite (5) |
|---|---|---|---|---|---|---|---|
| $SiO_2$ | 009 | 0.07 | 0.05 | 0.04 | 0.05 | 0.06 | 2.17 |
| MgO | 0.26 | 0.13 | 0.08 | 0.08 | 012 | 0.13 | 3.00 |
| CaO | n.d. | n.d. | n.d. | n.d | n.d | n.d | 0.30 |
| FeO | 31.96 | 32.10 | 32.30 | 32.57 | 32.54 | 32.29 | 28.87 |
| MnO | 0.64 | 0.77 | 0.78 | 0.69 | 0.73 | 0.72 | 0.92 |
| NiO | 0.04 | 0.07 | n.d | 0.07 | 0.06 | 0.05 | 0.08 |
| $Al_2O_3$ | n.d | n.d | n.d | 0.01 | n.d | n.d | 7.98 |
| $P_2O_5$ | n.d | 0.02 | n.d | n.d | n.d | n.d | n.d |
| $Cr_2O_3$ | 66.20 | 66.25 | 66.14 | 65.80 | 65.35 | 65.95 | 54.95 |
| $V_2O_3$ | 0.83 | 0.88 | 0.87 | 0.75 | 0.87 | 0.84 | 0.71 |
| $TiO_2$ | 0.21 | 0.09 | 0.02 | 0.03 | 0.06 | 0.08 | 1.16 |
| Total | 100.23 | 100.38 | 100.24 | 100.04 | 99.78 | 100.12 | 99.89 |

Number in parentheses = number of analyses; n.d. = not detected.

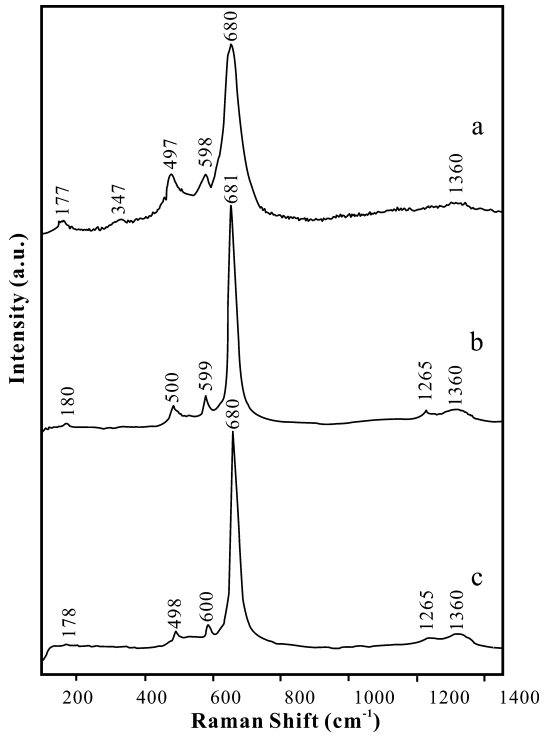


Fig. 11. Raman spectra of chromite. a) Al-rich chromite in the Yanzhuang chondritic host; b, c) Al-free chromite in the Yanzhuang nodule No.1.

of shock-damaged chromite in chondritic host. This also indicates that chromite in nodule No.1 is really a crystallized phase.

## DISCUSSION

The Yanzhuang meteorite underwent heterogenous shock compression in an asteroid impact event. It was estimated that the Yanzhuang chondritic host should have experienced shock pressures of 20–30 GPa and postshock temperatures of 150–350 °C (Chen and Xie 1996), while the chondritic melt pocket may have experienced shock pressures up to 50 GPa (based on the estimation of Stöffler et al. 1991), and postshock temperatures of about 2000 °C (Chen and Xie 1997).

Metal-troilite eutectic nodules are well developed in the chondritic melt pocket of the Yanzhuang meteorite, indicating in situ, closed system melting and a local Fe-Ni-S fractionation in the shock-induced melt. The Fe-Ni-S eutectic temperature is 950–1000 °C (Smith and Goldstein 1977).

The FeNi metal in nodule No.1 has higher contents of Ni and P and lower contents of Fe and Cr than the FeNi metal in the Yanzhuang chondritic host (Table 2). On the other hand, the troilite in nodule No.1 has higher contents of Fe, Ni, and Cr and lower contents of P, S, and Co than the troilite in the Yanzhuang chondritic host (Table 2). The P content in FeNi metal of the chondritic host is extremely low (0.01 wt%), but the P content in metal dendrites is higher (0.45–0.65 wt%). To the contrary, troilite in the chondritic host contains 1.10 wt% of P, but the troilite in nodule No.1 does not contain any P. This implies that phosphorous derived from phosphate was enriched in metal phase during the shock melting process.

Many of the Fe-Mn-Na phosphate globules and a number of Al-free chromite crystals were found within troilite in eutectic nodules, thus forming a distinct metal + troilite + Fe-Mn-Na phosphate + Al-free chromite assemblage in a H-type ordinary chondrite. The chemical compositions of phosphate globules in nodule No.1 resemble those of Fe-Mn-Na phosphates in the Yanzhuang eutectic nodules reported by Chen and Xie (1996), but the $Na_2O$ content of phosphates in nodule No.1 covers a wider range (from 0.75 to 6.65 wt%) than that of the phosphates (from 1.32 to 4.55 wt%) measured by Chen and Xie (1996). The $Na_2O$ content of 11 phosphate globules in nodule No.1 is higher than 4.62 wt% (Table 4). Hence, phosphates in this assemblage include Na-bearing graftonite, Mn-bearing galileiite, and a possible new phosphate phase of $Na_2(Fe,Mn)_{17}(PO_4)_{12}$ composition.

The predominate phosphate in the Yanzhuang chondritic host is whitlockite, $Ca_3(PO_4)_2$, which occurs as an accessory mineral and contains only up to 2.87 wt% $Na_2O$, while plagioclase in Yanzhuang contains 6.58 wt% $Na_2O$ (Chen 1992). However, our detailed microscopic observations could not find any whitlockite and plagioclase fragments in the melt regions of this meteorite. Also, no Mn minerals have been found in the Yanzhuang chondritic host, but olivine, low-Ca pyroxene, and chromite in it contain 0.46, 0.44, and 0.92 wt% of MnO, respectively (Table 1 and Table 5). On the other hand, the Mn contents of FeNi metal (0.09 wt%) and troilite (0.05 wt%) in Yanzhuang chondritic host are extremely low (Chen 1992). Our microprobe analyses reveal that the metal dendrites and the troilite in the metal-troilite-phosphates-chromite assemblage contain nearly undetectable Mn content (Table 2).

Olsen and Steele (1994) suggested a model to explain the formation of Fe-Mn-Na phosphates in some IIIAB iron meteorites: after Fe-phosphate formation, Mn, Na, K, and Ca diffuse into them forming Mn-bearing graftonite and 2:8:6 phosphate $(Na,K)_2(Fe,Mn)_8(PO_4)_6$. It seems that this model may be feasible for the case of iron meteorites that experienced very slow thermal metamorphism. However, it should be emphasized that the Fe-Mn-Na phosphates in Yanzhuang eutectic nodules were formed during a

shock event with a high cooling rate of shock-induced melt (Chen and Xie 1996).

Semeneko and Perron (2005) also found tiny phosphate globules and chromite crystals within troilite in the FeNi-FeS eutectic intergrowths in a melt region of the Krymka LL3.1 chondrite. They reported that quenching of the phosphate liquid resulted in the glassy globules in the troilite, and the composition of these phosphate globules is unusual, being Na-rich (7–11 wt% of $Na_2O$) and devoid of Ca. Besides the coarse euhedral crystals of chromite with variable composition in the troilite, they also found numerous euhedral chromite microcrystals within the glassy phosphate globules. They concluded that sulfur had not been largely lost but that a Fe-Ni-S melt formed large metal-troilite intergrowths. The Fe-Ni-S melt incorporated significant amounts of Na, which led to formation of a Fe-Na phosphate glass in troilite, with a composition close to that of maricite $NaFe_4(PO_4)_3$. Chromium partitioned into troilite rather than into metal and formed chromite crystals therein.

Although the phosphates within troilite in Krymka LL3.1 chondrite are glassy with a composition close to the Mn-free and Na-rich maricite, and both euhedral coarse-grained and microcrystalline chromites were observed in the melt region, we assume that their formation mechanism might be similar to that of Fe-Mn-Na phosphates and Al-free chromite within troilite in the Yanzhuang H6 chondrite.

As we mentioned before, the black melt veins and pockets of Yanzhuang have experienced shock pressures up to 50 GPa, and were heated to a peak temperature (approximately 2000 °C) similar to the melting point of refractory Al-rich chromite and olivine. Olivine, pyroxene, plagioclase, and whitlockite, as well as metal, sulfide, and chromite were melted after shock pressure release due to the very high postshock heat that brought the chondrite material above its liquidus. During cooling microcrystalline, olivine and pyroxene first crystallized from the chondritic melt, then metal-sulfide eutectic nodules and melt glass finally solidified at about 950–1000 °C.

Experiments by Urakawa et al. (1987) indicated that the oxygen solubility in the Fe-Ni-S system increases with pressure. The eutectic temperature in this Fe-Ni-S-O system is 900 °C. In the case of Yanzhuang, the volatile elements P and Na released from whitlockite and plagioclase along with element Mn and Cr released from chromite are concentrated into the shock-produced Fe-Ni-S-O liquid at high pressures and high temperatures. After pressure release, some P, on one hand, was partly combined with Fe, Mn, and Na in the Fe-Ni-S-O liquid to form Fe-Mn-Na phosphates, while on the other hand, part of P solidified in metal dendrites as solid solution (Chen et al. 1995a, 1995b).

The eutectic temperature (900 °C) in the Fe-Ni-S-O system is lower than the crystallization temperature of pyroxene and olivine in silica melt (1500 °C) (Chen et al. 1998). It shows that the metal-sulfide nodules were formed after solidification of the surrounding silicate melt. The FeNi metal-troilite-phosphate-chromite eutectic nodules show miscibility of a Fe-Ni-S-O-P system above 900 °C. When temperature drops below 900 °C, the Fe-Ni-S-O-P system becomes immiscible and segregates several kinds of melts including metal, sulfide, and phosphate. These melt pockets subsequently solidified into FeNi metal, troilite, and phosphates. As documented in this study, a number of rounded globules of phosphates occur as inclusions within sulfide (troilite).

It is clear from Table 1 that the concentration of $Cr_2O_3$ and $Al_2O_3$ in the pyroxene of Yanzhuang chondritic melt pocket (0.69 and 0.64 wt%) is higher than that associated with the host (0.14 and 0.20 wt%). As Cr is mainly hosted in chromite in equilibrated ordinary chondrites, chromite in the Yanzhuang chondritic melt pocket must have been melted during the shock event. Chromium released from chromite appears to partly enter the lattices of pyroxene during its recrystallization, and partly to concentrate into the Fe-Ni-S-O liquid. Chromium combines with Fe in liquid to form Al-free chromite. Aluminum released from chromite is mainly concentrated into recrystallized pyroxene in the chondritic melt pocket.

The above-described shock-induced phenomena in Yanzhuang melt regions may be of some geological and geochemical significance, as they provide a valuable natural example for understanding the fractionation and differentiation of the chondritic material in primitive Earth's mantle and the element redistribution between differentiated phases (1) under high pressure and high temperature, separation of FeNi metal from a silicate phase in the liquid state could take place to form FeNi liquid and silicate melt; (2) FeNi liquid could be the main source material of the Earth's core, and olivine and pyroxene recrystallized from separated silicate melt could be the main constituent minerals of the Earth's mantle, and the light silicate melt glass could be the source material of the Earth's crust; (3) FeS tents to combine with FeNi to form Fe-Ni-S liquid, and the oxyphile elements P and Na, as well as the siderophile elements Mn, and Cr, may concentrate into the Fe-Ni-S liquid, as these elements may show strong sulfophile properties under increased fugacity of sulfur; (4) the lithophile elements Si, Al, K, and Na are mainly concentrated into the glass phase, while a small portion of Al, Cr, Ca, and

Na is combined with pyroxene recrystallized from silicate melt.

## CONCLUSION

1. The occurrence of metal + troilite + Fe-Mn-Na phosphates + Al-free chromite assemblage was identified in a large metal-troilite eutectic nodule in the chondritic melt pocket of the heavily shocked Yanzhuang H6 chondrite.
2. A few phosphate globules have the composition of a Na-bearing graftonite $(Fe,Mn,Na)_3(PO_4)_2$, and the majority of them correspond to two phosphate minerals: Mn-bearing galileiite $Na(Fe,Mn)_4(PO_4)_3$ and a possible new phosphate phase of $Na_2(Fe,Mn)_{17}(PO_4)_{12}$ composition.
3. All minerals in the Yanzhuang melt regions were melted after pressure release to form a chondritic melt due to the very high postshock heat that brought the chondrite material above its liquidus. The volatile elements P and Na released from whitlockite and plagioclase along with element Cr and Mn released from chromite are concentrated into the shock-produced Fe-Ni-S-O liquid at high temperatures.
4. During cooling, microcrystalline olivine and pyroxene first crystallized from the chondritic melt, then metal-troilite eutectic intergrowths and silicate melt glass finally solidified at about 950–1000 °C, while P, Mn, and Na in the Fe-Ni-S-O liquid combined with Fe and crystallized as Fe-Mn-Na phosphates within troilite, and Cr combined with Fe and crystallized as Al-free chromite also within troilite.

*Acknowledgments*—This work was supported by National Natural Science Foundation of China (Grant No. 41172046 for Xie and grant No. 41372040 for Zhai). We thank Chen Linli and Tan Daying for assistance with the electron microprobe and Raman spectroscopic analyses, respectively. We are grateful to E. Walton and M. Ebert for their thorough and constructive reviews, which helped to improve the manuscript considerably.

*Editorial Handling*—Dr. Wolf Reimold

## REFERENCES

Antenucci D., Miehe G., Tarte P., Schemahl W. W., and Fronsolet A. M. 1993. Combined X-ray Rietveld, infrared and Raman study of a new synthetic variety of alluaudite, $NaCdIn_2(PO_4)_3$. *European Journal of Mineralogy* 5:207–213.

Begemann F. and Wlotzka F. 1969. Shock induced thermal metamorphism amd mechanical deformation in the Ramsdorf chondrite. *Geochimica et Cosmochimica Acta* 33:1351–1370.

Begemann F., Palme H., Spettel B., and Weber H. W. 1992. On the thermal history of heavily shocked Yanzhuang H-chondrite. *Meteoritics* 27:174–178.

Bild R. W. 1974. New occurrences of phosphates in iron meteorites. *Contributions to Mineralogy and Petrology* 45:91–98.

Burba C. M. and Frech R. 2006. Vibrational spectroscpic investgation of structurally related $LiFePO_4$, $NaFePO_4$, $FePO_4$, compounds. *Spectrochimica Acta, Part A* 65:44–50.

Chen M. 1992. Micromineralogy and shock effects in Yanzhuang chondrite (H6). Ph.D. thesis, The Institute of Geochemistry, Chinese Academy of Sciences. 95 p.

Chen M. and Xie X. 1995. TEM microstructures of the metallic dendrites in the shock-induced melt pocket of the Yanzhuang meteorite. *Neues Jahrbuch fur Mineralogie—Abhandlungen* 8:337–343.

Chen M. and Xie X. 1996. Na behavior in shock-induced melt phase of the Yanzhuang (H6) chondrite. *European Journal of Mineralogy* 8:325–333.

Chen M. and Xie X. 1997. Shock effects and history of the Yanzhuang meteorite: A case different from the L-chondrites. *Chinese Science Bulletin* 42:1889–1893.

Chen M., Xie X., and El Goresy A. 1995a. Nonequilibrium solidification and microstructures of metal phases in the shock-induced melt of the Yanzhuang (H6) chondrite. *Meteoritics* 30:28–32.

Chen M., Wopenka B., Xie X., and El Goresy A. 1995b. A new high-pressure polymorph of chlorapatite in the shocked Sixiangkou (L6) chondrite. Proceedings, 26th Lunar and Planetary Science Conference. pp. 237–238.

Chen M., Sharp T. G., El Goresy A., Wopenka B., and Xie X. 1996. The majorite - pyrope + magnesiowustite assemblage: Constraints on the history of shock veins in chondrites. *Science* 271:1570–1573.

Chen M., Xie X., and El Goresy A. 1998. Olivine plus pyroxene assemblages in shock veins of the Yanzhuang chondrite: Constraints on the history of H-chondrite. *Neues Jahrbuch fur Mineralogie—Abhandlungen* 3:97–110.

Chen M., Xie X., Wang D., and Wang S. 2002. Metal-troilite-magnetite assemblage in shock veins of Sixiangkou meteorite. *Geochimica et Cosmochimica Acta* 66:3143–3149.

Chen M., Shu J., Xie X., and Mao H.-K. 2003a. Natural $CaTi_2O_4$-structured $FeCr_2O_4$ polymorph in the Suizhou meteorite and its significance in mantle mineralogy. *Geochimica et Cosmochimica Acta* 67:3937–3942.

Chen M., Shu J., Mao H.-K., Xie X., and Hemley R. J. 2003b. Natural occurrence and synthesis of two new postspinel polymorphs of chromite. *Proceedings of the National Academy of Sciences* 100:14651–14654.

Downs R. T. 2006. The RRUFF Project: An integrated study of the chemistry, crystallography, Raman and infrared spectroscopy of minerals. Program and Abstracts of the 19th General Meeting of the International Mineralogical Association in Kobe, Japan. 03-13.

Fredriksson K., DeCarli P. S., and Aaramäe A. 1963. Shock induced veins in chondrites. In *Space research III*, edited by Priester W. Amsterdam, the Netherlands: North-Holland. pp. 973–983.

Fuchs L. H. 1969. The phosphate mineralogy of meteorites. In *Meteorite research*, edited by Millman P. M. Dordrecht, the Netherlands: D. Reidel Pub. Co. pp. 683–695.

Gillet P., Chen M., Dubrovinsky L., and El Goresy A. 2000. Natural $NaAlSi_3O_8$ –hollandite in the Sixiangkou meteorite. *Science* 287:1633–1637.

Kong P. and Xie X. 2003. Redistribution of elements in the heavily shocked Yanzhuang chondrite. *Meteoritics & Planetary Science* 38:739–746.

Leroux H., Doukhan J. C., and Guyot F. 2000. Metal-silicate interaction in quenched shock-induced melt of the Tenham L6-chondrite. *Earth and Planetary Science Letters* 179:477–487.

Lodziński M. and Sitarz M. 2009. Chemical and spectroscopic characterization of some phosphate accessory minerals from pegmatites of the Sowie Góry Mys, SW Poland. *Journal of Molecular Structure* 924–926:442–447.

Olsen E. J. and Fredriksson K. 1966. Phosphates in iron and pallasite meteorites. *Geochimica et Cosmochimica Acta* 30:459–470.

Olsen E. J. and Steele I. M. 1993. New alkali phosphates and their associations in the IIIAB iron meteorites. *Meteoritics* 28:415.

Olsen E.J. and Steele I.M. 1994. Lithophile element diffusion profiles in phosphate phases in IIIAB iron meteorites: A clue to the trace lithophiles in metal during core formation. Proceedings, 25th Lunar and Planetary Science Conference. pp. 1025–1026.

Olsen E. J. and Steele I. M. 1997. Galileiite: A new meteoritic phosphate mineral. *Meteoritics & Planetary Science* 32: A155–A156.

Price G. D., Putnis A., and Agrell S. 1979. Electron petrography of shock-produced veins in the Tenham chondrite. *Contributions to Mineralogy and Petrology* 71:211–218.

Rubin A. E. 1985. Impact melt products of chondritic material. *Reviews of Geophysics* 23:277–300.

Rubin A. E. 1997. Mineralogy of meteorite groups. *Meteoritics & Planetary Science* 32:231–247.

Scott E. R. D. 1982. Origin of rapidly solidified FeNi-FeS grains in chondrites and iron meteorites. *Geochimica et Cosmochimica Acta* 46:813–823.

Semeneko V. P. and Perron C. 2005. Shock-melted material in the Krymka LL3.1 chondrite: Behavior of the opaque minerals. *Meteoritics & Planetary Science* 40:173–185.

Sharp T. G., Lingemann C. M., Dupas C., and Stöffler D. 1997. Natural occurrence of $MgSiO_3$- ilmenite and evidence for $MgSiO_3$–perovskite in a shocked L chondrite. *Science* 277:352–255.

Smith B. A. and Goldstein J. I. 1977. The metallic microstructures and thermal histories of severely reheated chondrites. *Geochimica et Cosmochimica Acta* 44:1062–1072.

Stöffler D., Keil K., and Scott E. R. D. 1991. Shock metamorphism of ordinary chondrites. *Geochimica et Cosmochimica Acta* 55:3845–3867.

Taylor G. J. and Heymann D. 1971. Postshock thermal history of reheated chondrites. *Journal of Geophysical Research* 76:1879–1893.

Urakawa S., Kato M., and Kumazawa M. 1987. Experimental study on the phase relations in the system Fe-Ni-O-S up to 15 GPa. In *High pressure research in mineral physics*, edited by Manghnani M. H. and Syono Y. Tokyo, Japan: Terra Science. pp. 95–111.

Xie X., Li Z., Wang D., Liu J., Hu R., and Chen M. 1991. The new meteorite fall of Yanzhuang, a severely shocked H6 chondrite with black molten materials. *Meteoritics* 26:411.

Xie X., Li Z., Wang D., Liu J., Hu R., and Chen M. 1994. The new meteorite fall of Yanzhuang, a severely shocked H6 chondrite with black molten materials. *Chinese Journal of Geochemistry* 12:39–46.

Xie X., Chen M., Dai C., El Goresy A., and Gillet P. 2001. A comparative study of naturally and experimentally shocked chondrites. *Earth and Planetary Science Letters* 187:345–356.

Xie X., Minitti M. E., Chen M., Wang D., Mao H.-K., Shu J., and Fei Y. 2002. Natural high-pressure polymorph of merrillite in the shock vein of the Suizhou meteorite. *Geochimica et Cosmochimica Acta* 66:2439–2444.

Xie X., Sun Z., and Chen M. 2011. The distinct morphological and petrological features of shock melt veins in the Suizhou L6 chondrite. *Meteoritics & Planetary Science* 46:459–469.

Xie X., Zhai S., Chen M., and Yang H. 2013. Tuite, $\gamma$-$Ca_3(PO_4)_2$, formed by chlorapatite decomposition in a shock vein of the Suizhou L6 chondrite. *Meteoritics & Planetary Science* 48:1515–1523.